Computational Particle Mechanics
https://doi.org/10.1007/s40571-022-00484-8

Statistical modelling and optimization of AL/CNT composite using response surface-desirability approach

M. Motamedi[1] · **A. Mehrvar**[1] · **M. Nikzad**[1]

Received: 2 April 2022 / Revised: 20 May 2022 / Accepted: 21 May 2022

Abstract
Nowadays, various methods are being formed on new composites and nanocomposite compounds. Investigating the properties of nanocomposites and finding their optimal properties pave the way for a better use of them. In this study, first, mechanical molecular dynamics method is used to investigate mechanical properties of aluminum/carbon nanotubes (Al-CNT) nanocomposite, then, the effect of temperature change, strain rate, and chirality of nanotubes on the elastic modulus and ultimate stress of nanocomposite have been investigated. However, in order to simultaneously investigate these three parameters on the properties of nanocomposite and to find an optimal point for the elastic modulus and ultimate stress, the experimental design method for optimization was used. Derringer method was used to determine optimal parameters for simultaneous optimization of two response variables, namely elastic modulus and ultimate stress. It can be concluded that the optimal conditions occur simultaneously at 50 K, strain rate 0.01, and chirality (5,5), in which the value of the elastic modulus is 156 GPa and the ultimate strain value is 13.7 GPa and simultaneous minimum value of elastic modulus and ultimate stress occur at 650 K, strain rate 0.0205, chirality (3,3), in which the value of elastic module is 94 GPa and the ultimate strain value is 6.44 GPa.

Keywords Nanocomposites · Optimization · Response surface methodology · Mechanical properties

1 Introduction

Nowadays, many developments are taking place in the field of new materials such as composites [1]. Different studies are done on new composite and nanocomposite compounds. In the nano dimension, extensive studies are being conducted with new nanotechnology methods [2]. Nanocomposites are high-performance materials which are a combination of unusual features and a unique design, and with an annual growth rate of about 25%, they have great potential for a variety of applications [3]. Nanocomposites have practical properties. The use of nanocomposites in material processing can result in the production of single-phase or multi-phase ceramics and porous materials with special properties [4]. In recent years, due to the different mechanical properties of CNTs, carbon nanotube reinforced metal composites have attracted the attention of many scientists and researchers [5–14]. Aluminum/carbon nanotubes composite is one of the most popular metal composites that has been discussed and studied in recent years [15]. Using ball milling, Esawi et al. [16] combined 2 wt. % carbon nanotubes in aluminum, which increased the tensile strength of aluminum by 21%. Aluminum/carbon nanotubes composite as a combination of powder metallurgy and subsequent friction stir processing (FSP) was made by Liu et al. [17], and the microstructural observations showed that carbon nanotubes were dispersed separately in the composites and that the carbon nanotubes tended to disperse between the grain boundaries. Although carbon nanotubes were shortened and some Al4C3 was formed in the matrix, the layered structures of carbon nanotubes were well preserved. Friction and wear characteristics of carbon nanotubes composites were evaluated by Kim et al. [18] based on the conditions of dispersion rate, fabrication method, and amount of carbon nanotubes in composites. Mechanical and thermal properties of aluminum/carbon nanotubes composites were investigated by Jianhua Wu et al. [19] Aluminum composites reinforced with 0–5.0 wt.% multi-walled carbon nanotubes, were produced by spark plasma sintering (SPS) method. A maximum thermal conductivity

✉ M. Motamedi
motamedi@shahreza.ac.ir

[1] Department of Mechanical Engineering, Shahreza Campus, University of Isfahan, Isfahan, Iran

Published online: 14 June 2022

of 199 W/ m/ K and a maximum tensile strength of 130 MPa were observed in 0.5 wt. % multi-walled aluminum/carbon nanotube composite. The results indicated that multi-walled carbon nanotube aluminum matrix composite is a suitable material for applications with high thermal conductivity. Chen et al. [20] reported that aluminum/carbon nanotube composite have better ductility when they have higher tensile strength. Izadi et al. [21] used multi-pass friction stir processing to produce aluminum/ multi-walled carbon nanotube composite. The hardness of these composites was found to be twice as high as the original alloy.

Liu et al. [22] analyzed shortening of the carbon nanotubes and strength of the composites in aluminum/carbon nanotube composite, produced by multi-pass friction stir processing. The carbon nanotubes dispersed in an aluminum matrix with 4.5 vol.% CNT. This model indicated that change in length of carbon nanotubes has a linear relationship with the mechanical properties of the composite. Tensile strength data obtained from aluminum/carbon nanotube composite were analyzed by Bakshi et al. [23] to investigate effects of carbon nanotube dispersion and its volume fraction on the elastic modulus, strength, and hardness of composites, and the highest strength was obtained for carbon nanotubes with a volume fraction of less than 2 vol.%. Also, tensile data in magnesium/carbon nanotube composite and copper/carbon nanotubes were compared with aluminum carbon nanotube composite, and the results indicated that the reinforcement is not effective when there is no chemical interaction between the metal matrix and the carbon nanotube. Salama et al. [24] introduced a microstructural design of aluminum/carbon nanotube composite to improve ductility. It was indicated that dual matrix structure composites have about 14.8% more ductility compared to single matrix structure composites. Hassan et al. [25] investigated the effect of carbon nanotube damage on the mechanical properties of aluminum/carbon nanotube composite by using damaged carbon nanotubes, and it was found that the composites made of damaged carbon nanotube have 97.5% higher strength and 14.2% higher modulus than pure aluminum. Park et al. [26] studied strengthening mechanisms in aluminum/carbon nanotube composite and found that yield strength and tensile strength of aluminum/carbon nanotube composite improved by 60% and 23%, respectively. However, since experimental studies are time-consuming and costly, molecular dynamics simulations have been used to stimulate atomic structures and predict the mechanical properties of various nanocomposites, including carbon nanotube-metal nanocomposite. Yan et al. [27] used molecular dynamics method to study the tensile responses of copper/carbon nanotube nanocomposite. The results indicated that carbon nanotubes have a significant reinforcing effect on Young's modulus and yield strength of copper/carbon nanotube nanocomposite, and with increasing number of carbon nanotubes, the Young's modulus of the nanocomposite increases linearly. Also, Motamedi et al. [28–30] investigated the mechanical properties of Al/CNT nanocomposite, using molecular dynamics method as well as continuum model of composite and finite element method. They have also used molecular dynamics method to predict mechanical properties of other nanostructures. Silvestre et al. [31] studied the compressive behavior of carbon nanotubes reinforced aluminum composites by using molecular dynamics method, in which a carbon nanotube (6–6) is used inside an aluminum box, and the Young's modulus of composite increased more than 60% compared to pure aluminum.

This study has two parts. In the first part, the mechanical properties of Al/CNT nanocomposite will be obtained by molecular dynamics method. Then, the effects of temperature, strain rate and chirality on the behavior of the stress–strain curve will be investigated. In the second part, nanocomposites will be optimized by using experimental design method and using the three input parameters of temperature, strain rate, and chirality, and the optimal and minimum values for the elastic modulus and the ultimate stress will be obtained.

2 Computational approach

2.1 Molecular dynamics simulation

The Molecular dynamics simulation was done by rectangular box of aluminum and a single-walled carbon nanotube (SWCNT) which is introduced as representative volume element (RVE). The size of aluminum box is 46 Å *46 Å *93 Å and has 12,167 atoms. The CNTs with different chiralities have been used in Al matrix. The first CNT has zigzag (3,3) configuration with length 93 Å and 456 atoms. The second one has zigzag (4,4) configuration with length 93 Å and 608 atoms. The third has zigzag (5,5) configuration with length 93 Å and 760 atoms. The fourth one (6,6) has 912 atoms, and The last one has zigzag (7,7) configuration with length 93 Å and 1064 atoms.

2.2 Interatomic Potentials

There are numerous potential possibilities which can be utilized for nanocomposites. For this demonstrate, there are three sorts of potential possibilities, Al-Al interaction, Carbon–Carbon interaction, and Al-Carbon interaction.

AIREBO potential [32] and REBO potential [33] were used for calculating the potential energy and the interatomic force:

$$E = \frac{1}{2}\sum_{i}\sum_{j\neq i}\left(E_{ij}^{REBO} + E_{ij}^{LJ} + \sum_{k\neq i,\,j}\sum_{l\neq i,\,j,\,k} E_{kijl}^{tors}\right) \quad (1)$$

The first and second terms are REBO and Lennard Jones potential, respectively. The third term is:

$$E_{ijkl}^{tors} = f_c(r_{ij}) f_c(r_{ik}) f_c(r_{jl}) \varepsilon \left[\frac{256}{405} cos^{10}\left(\frac{\varphi}{2}\right) - 0.1 \right] \quad (2)$$

where ϕ, f_c, ε are angle, bond-weight parameter, and Lennard–Jones parameter.

For aluminum-aluminum interaction, EAM potential was used [24, 25]:

$$E_i = F_\alpha \left(\sum_{j \neq i} \rho_\beta (r_{ij}) \right) + \frac{1}{2} \sum_{j \neq i} \phi_{\alpha\beta}(r_{ij}) \quad (3)$$

r_{ij}, $\emptyset_{\alpha\beta}$, ρ_β, F_α , are atoms distance, potential function in pairs, electron charge density, and embedding function, respectively.

The Lennard–Jones function was used for aluminum- carbon nanotube interaction:

$$E = 4\varepsilon \left[\left(\frac{\sigma}{r}\right)^{12} - \left(\frac{\sigma}{r}\right)^{6} \right] \quad (4)$$

ε is the depth of the potential well, and σ is the distance at which the particle–particle potential energy E is zero.

2.3 Simulation terms and conditions

Using NPT ensemble, the Equilibration was done in 1 ns with the time step of 1 fs, in 50, 100, 273, 300, 350, 400, 450, 500, 600 K, and 1 bar pressure.

In the MD simulation step (tensile load), the RVE was pulled in the direction of the RVE axis with strain rates of 10^{-5}/ps, 10^{-4}/ps, 10^{-3}/ps, 10^{-2}/ps, 3×10^{-2}/ps, 5×10^{-2}/ps, 7×10^{-2}/ps and 9×10^{-2}/ps. Figure 1 presents pulling simulation of nanocomposite.

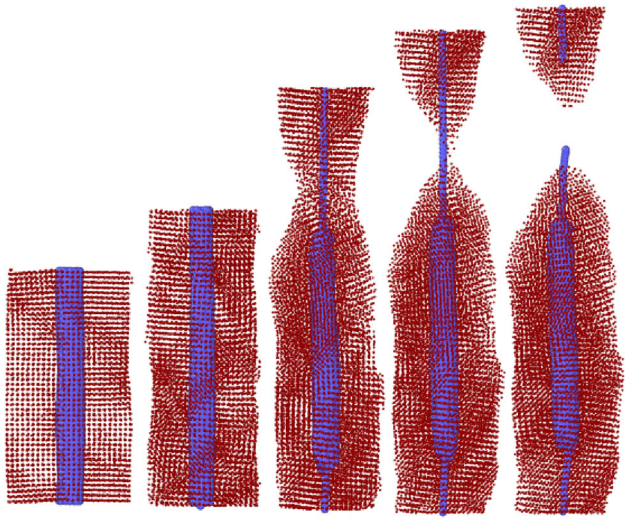

Fig. 1 Pulling simulation of nanocomposite

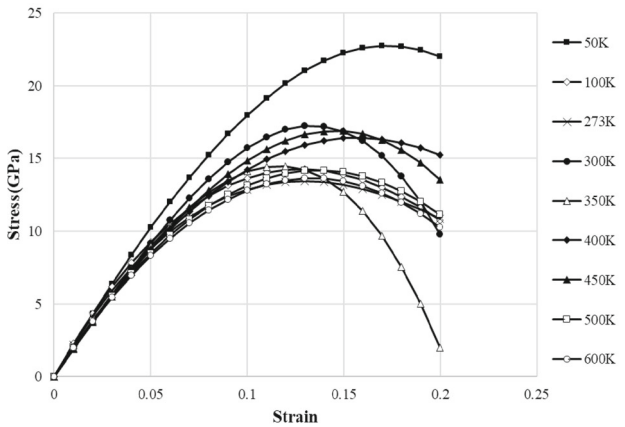

Fig. 2 Effect of temperature on stress–strain diagram

3 Results and discussion

First, to ensure the method, the stress–strain diagram of pure aluminum was examined with aforementioned conditions, by the molecular dynamics method. Then, the results were compared with previous works. In two different cases, case A of completely free carbon nanotube and case B with fixed CNT, it was shown that the Young's modulus of nanocomposites increased by 50% compared to the Young's modulus of pure aluminum. In other work, the results illustrated that the Young's modulus of aluminum-carbon nanotube composites with chiralities of (4,4), (6,6), and (8,8) in comparison to the amount of Young's modulus obtained for pure Al, increased by 31%, 33%, and 39%, respectively [34–40]. In our work, a significant increase in the amount of Young's modulus compared to pure aluminum was also observed.

3.1 Investigating the effect of different parameters

3.1.1 Investigating the effect of temperature

First, the effect of temperature on the stress–strain curve of aluminum carbon nanotube nanocomposite was investigated. For this purpose, temperatures of 50, 100, 273, 300, 350, 400, 450, 500, and 600 K were used in simulation. The chirality of the nanotube (6,6) is also considered. The system pressure was 100 kPa and the strain rate was 0.0001/ps. The stress–strain diagram is shown in Fig. 2.

The Young's modulus value of the materials can be obtained by using the slope of the stress–strain diagram in the elastic region. The ultimate stress value can also be

Table 1 The Young's modulus of Al/CNT nanocomposite for different temperatures

Temperature (K)	50	100	273	300	350	400	450	500	600
Elastic modulus (GPa)	210	198.13	188.74	186.55	185.01	183.78	180.35	178.94	176.27
Ultimate stress (GPa)	22.73	14.25	13.437	17.25	14.491	16.42	16.898	14.181	13.97

obtained from the stress–strain diagram. For the above values, the value of the Young's modulus and the ultimate stress is extracted and shown in Table 1.

According to the results, the Young's modulus of the nanocomposite decreases with increasing temperature. This result is consistent with the results of Bayer's experimental work [41] and Singh's simulation work [42].

But, no special trend is observed with increasing temperature for the ultimate stress value. But, it is clear that at 50 K, the stress–strain diagram will be more inclined, due to the extreme brittleness of the material. Therefore, the value of ultimate stress will be more than the material in the ductile state.

3.1.2 Investigating the effect of strain rate

One of the most important parameters in the tensile test is the strain rate. In general, the strain value is obtained from the following equation:

$$\in (t) = \frac{L(t) - L_0}{L_0} \tag{5}$$

where L_0 is the original length and $L(t)$ is length at each time t. Then the strain rate will be:

$$\dot{\in}(t) = \frac{\mathrm{d} \in}{\mathrm{d}t} = \frac{\mathrm{d}}{\mathrm{d}t}\left(\frac{L(t) - L_0}{L_0}\right) = \frac{1}{L_0}\frac{\mathrm{d}L(t)}{\mathrm{d}t} = \frac{v(t)}{L_0} \tag{6}$$

where $v(t)$ is the speed at which the ends are moving away from each other.

Figure 3 shows the stress–strain diagram of the nanocomposite for different strain rates. In this case, the chirality of the carbon nanotube (6,6) at a pressure of 100 kPa and at a temperature of 273 K is considered.

The Young's modulus and the ultimate stress of the nanocomposite are obtained from the stress–strain diagrams in Fig. 3, the values of which are presented in Table 2.

As can be seen in Fig. 3 and Table 2, by increasing the strain rate from 0.00001/ps to 0.09/ps the Young's modulus decreased by 31%, which is a significant value. This indicates that in molecular dynamics simulations, the strain rate parameter is one of the most significant and influential parameters in the results.

Jun Hua et al. [43] investigated the effect of strain rate on the Young's modulus of copper nanocomposite. The results

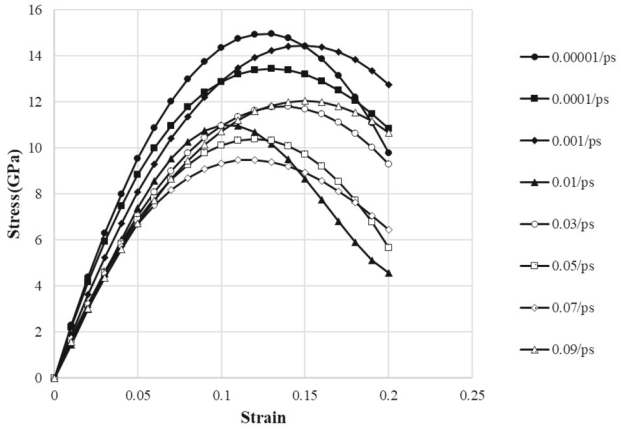

Fig. 3 The stress–strain diagram of nanocomposite for different strain rates

showed that by increasing the strain rate from 0.0005/ps to 0.005/ps, the Young's modulus decreased from 210 to 191GPa (about 9%). In the present study, with the same order, if the strain rate changes from 0.0001/ps to 0.001/ps, the Young's modulus will decrease by about 10%, which shows a good agreement. Also, Moeini et al. [44] indicated that increasing strain rate decreases the Young's modulus of nanocomposites.

3.1.3 Investigating the effect of chirality

In order to investigate the effect of chirality on the mechanical properties of nanocomposite, nanotubes with different chiralities were studied. The chirality is zigzag type. In this case, the stress–strain diagram for temperature 273 K and pressure 100 kPa, and stress rate 0.01/ps is shown in Fig. 4. Also, the Young's modulus and the ultimate stress for this case are shown in Table 3.

As expected, by increasing chirality, which in turn increases the diameter, the Young's modulus value of nanocomposite will be increased. The reason is increasing the volume ratio of nanotubes in the composite, which due to the fact that nanotubes have high strength; therefore, it will have a more effect on the Young's modulus of the nanocomposite. According to the relationships between the composites, they represent volume of the composite V_{RVE} is equal to [31]:

$$V_{RVE} = V_{Al} + V_{CNT} \tag{7}$$

Table 2 The Young's modulus of Al/CNT nanocomposite for different strain rates

Strain rate (1/ps)	0.00001	0.0001	0.001	0.01	0.03	0.05	0.07	0.09
Elastic modulus (GPa)	202.4	188.74	169.57	149.4	147.89	145.42	142.98	139.99
Ultimate stress (GPa)	14.963	13.437	14.44	10.99	11.8	10.39	9.478	12.04

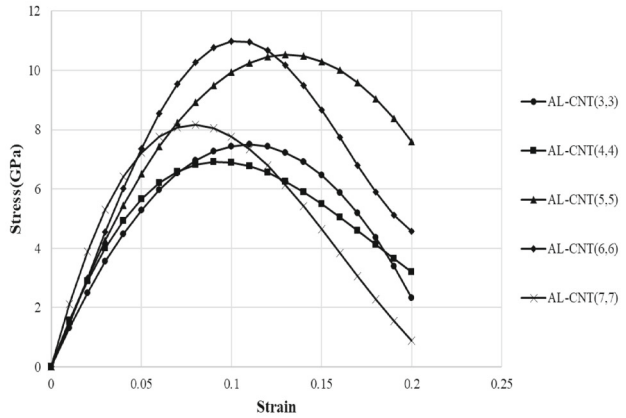

Fig. 4 The stress–strain diagram of nanocomposite for different chiralities

Silvestre [31] used elasticity theory to predict composite elasticity. is:

$$Y_{RVE} = V_{CNT}Y_{CNT} + V_{Al}Y_{Al} \tag{8}$$

which V_{CNT} and V_{Al} are volume of carbon nanotube and aluminum, and Y_{CNT} and Y_{Al} are Young's modulus of carbon nanotube and aluminum. It is clear that, as the volume percentage of nanotubes increases; which is due to the increase in chirality, we expect the Young's modulus to increase, too.

3.2 Statistical modeling and optimization

In the design of experiments, changes are consciously made in the process input variables, in order to observe and identify the amount of changes in the output response of the process [45, 46]. The process in this research is a combination of factors and parameters studied in the previous section, the output of which is to improve the mechanical properties. In this study, temperature, strain rate, and chirality were considered as the input parameters while ultimate stress (*Sut*) and the Young's modulus (E) were considered as the output parameters. Also, response surface methodology (RSM) was applied as a design of experiment (DOE) method, and Minitab software has been used to execute it.

The experimentation strategy was used based on the Box-Behnken design. The temperature and strain rate parameters are considered in five levels, and the chirality parameter is considered in three types. Input parameters and their levels are presented in Table 4. According to the number of input parameters and the experimentation strategy, the number of simulation runs in the software is 39 run.

Table 5 presents the values of response variables for the 39 numerical simulations performed.

3.2.1 The mathematical modeling of the ultimate stress using the RSM

The results of the analysis of variance (ANOVA) related to the ultimate stress are presented in Table 5. As a result, and the quadratic mathematical model in terms of encoded input parameters for the response variable of the ultimate stress is as follows:

$$\begin{aligned} Sut &= 11.17 - 0.01793T + 2.0S + 0.000015T * T - 48 \\ &\quad S * S + 0.0441T * S \\ Sut &= 12.66 - 0.01921T + 2.5S + 0.000015T * T - 48 \\ &\quad S * S + 0.0441T * S \\ Sut &= 14.87 - 0.02174T - 12.4S + 0.000015T * T - 48 \\ &\quad S * S + 0.0441T * S \end{aligned} \tag{9}$$

where T is the temperature in Kelvin and S is the strain rate in picoseconds. *Sut* is the ultimate stress in GPa. The above three equations are for type 1 to type 3 chirality, respectively. As can be seen in Eq. 9, the ultimate stress values for each chirality can be obtained as a function of temperature and strain rate.

Table 3 The Young's modulus of Al/CNT nanocomposite for different chiralities

Chirality of CNT (nm)	(3,3)	(4,4)	(5,5)	(6,6)	(7,7)
Elastic modulus (GPa)	112.59	124.2	136.65	149.4	161.93
Ultimate stress (GPa)	7.498	6.914	10.52	10.981	8.161

Table 4 Input parameters and their levels

Input parameters	Levels				
	− 2	− 1	0	1	2
Temperature T (K)	50	200	350	500	650
Strain rate S (1/ps)	0.01	0.03	0.05	0.07	0.09
Chirality C (nm)	3 types: (3,3), (4,4), (5,5)				

Table 5 The values of response variables

Run order	Temperature T (K)	Strain rate S (1/ps)	Chirality C	Elastic modulus E (GPa)	Ultimate stress Sut (GPa)
1	350	0.05	(3,3)	103.44	7.648
2	500	0.03	(5,5)	121.19	8.274
3	650	0.05	(4,4)	105.33	7.493
4	350	0.05	(4,4)	115.64	8.667
5	650	0.05	(3,3)	93.61	6.444
6	350	0.05	(3,3)	103.44	7.648
7	350	0.09	(5,5)	124.17	9.399
8	350	0.05	(3,3)	103.44	7.648
9	500	0.07	(3,3)	92.79	7.591
10	350	0.01	(4,4)	119.17	7.779
11	350	0.05	(5,5)	127.41	9.113
12	50	0.05	(5,5)	150.64	14.743
13	350	0.05	(5,5)	127.41	9.113
14	350	0.05	(5,5)	127.41	9.113
15	200	0.07	(5,5)	135.44	9.259
16	200	0.03	(3,3)	114.06	7.858
17	350	0.05	(5,5)	127.41	9.113
18	350	0.01	(5,5)	131.22	9.106
19	500	0.07	(4,4)	106.85	8.674
20	350	0.09	(4,4)	111.56	9.029
21	350	0.05	(4,4)	115.64	8.667
22	350	0.09	(3,3)	99.95	7.934
23	350	0.05	(3,3)	103.44	7.648
24	200	0.07	(4,4)	123.82	9.093
25	350	0.05	(4,4)	115.64	8.667
26	500	0.03	(3,3)	97.36	6.843
27	350	0.05	(4,4)	115.64	8.667
28	500	0.03	(4,4)	108.87	7.684
29	200	0.07	(3,3)	111.12	8.866
30	500	0.07	(5,5)	117.77	8.031
31	350	0.05	(5,5)	127.41	9.113
32	650	0.05	(5,5)	113.36	8.065
33	50	0.05	(3,3)	124.08	10.034
34	50	0.05	(4,4)	137.88	12.292
35	350	0.05	(4,4)	115.64	8.667

Table 5 (continued)

Run order	Temperature T (K)	Strain rate S (1/ps)	Chirality C	Elastic modulus E (GPa)	Ultimate stress Sut (GPa)
36	200	0.03	(5,5)	140.79	10.015
37	350	0.01	(3,3)	107.59	7.29
38	200	0.03	(4,4)	128.56	9.436
39	350	0.05	(3,3)	103.44	7.648

Table 6 Analysis of Variance for the ultimate stress

Source	DF	Adj SS	Adj MS	F-value	P-value
Model	11	69.8279	6.3480	19.72	0.000
Linear	4	58.1393	14.5348	45.16	0.000
T	1	39.1959	39.1959	121.77	0.000
S	1	0.9274	0.9274	2.88	0.101
C	2	18.0160	9.0080	27.99	0.000
Square	2	8.7659	4.3830	13.62	0.000
T*T	1	7.7833	7.7833	24.18	0.000
S*S	1	0.0251	0.0251	0.08	0.782
2-Way Interaction	5	2.9226	0.5845	1.82	0.143
T*S	1	0.2096	0.2096	0.65	0.427
T*C	2	2.0287	1.0144	3.15	0.059
S*C	2	0.6843	0.3422	1.06	0.359
Error	27	8.6908	0.3219		
Total	38	78.5187			
$R^2 = 88.93\%$, R^2 (adj) $= 84.42\%$					

According to the analysis of variance, the probability value is significantly less than 0.05, which indicates the adequacy of the model in the 95% confidence interval. In addition, the correlation coefficients R^2 and R^2adj for the ultimate stress model are 88.93% and 84.42%, respectively, ensuring an excellent fitting for the model.

3.2.2 The mathematical modeling of the Young's modulus using the RSM

The ANOVA details of the Young's modulus are shown in Table 7. According to this ANOVA results, the mathematical model of the Young's modulus is given in Eq. 10:

$$\begin{aligned} E &= 135.43 - 0.09873\,T - 130.1\,S + 0.000059\,T*T \\ &\quad + 58\,S*S + 0.0839\,T*S \\ E &= 148.89 - 0.10194\,T - 126.7\,S + 0.000059\,T*T \\ &\quad + 58\,S*S + 0.0839\,T*S \\ E &= 162.68 - 0.10754\,T - 130.4\,S + 0.000059\,T*T \\ &\quad + 58\,S*S + 0.0839\,T*S \end{aligned} \tag{10}$$

where T is the temperature in Kelvin and S is the strain rate in picoseconds. E is the Young's modulus in GPa. As can be seen in Eq. 10, the Young's modulus values for each chirality can be obtained as a function of temperature and strain rate.

According to the results of analysis of variance, the probability value of the Young's modulus model is significantly less than 0.05, which is desirable. Also, the values of correlation coefficients R^2 and R^2adj for this model are 99.78% and 99.69%, respectively; all of which indicate the adequacy and accuracy of the model.

3.2.3 The effect of input parameters on the ultimate stress and the Young's modulus

According to Table 6, the linear and quadratic terms obtained for the ultimate stress have the greatest effect on this output. In fact, according to the analysis of variance and considering P-value and F-value, linear terms and quadratic terms of temperature, and linear term of chirality have the greatest impact on the ultimate stress. Also, Fig. 5 shows that the ultimate stress increases with decreasing temperature, increasing the strain rate, and considering the third type of chirality.

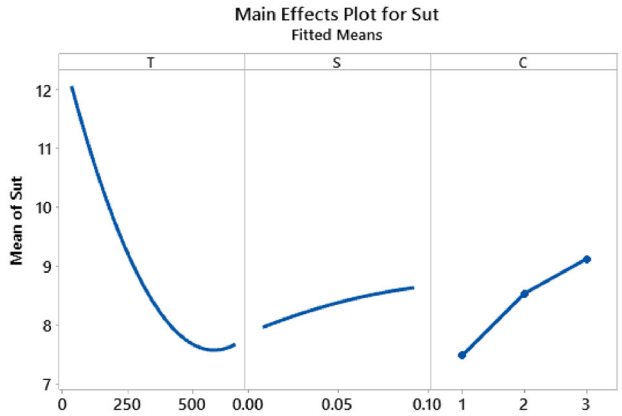

Fig. 5 Effect of temperature, strain rate, and chirality on ultimate stress

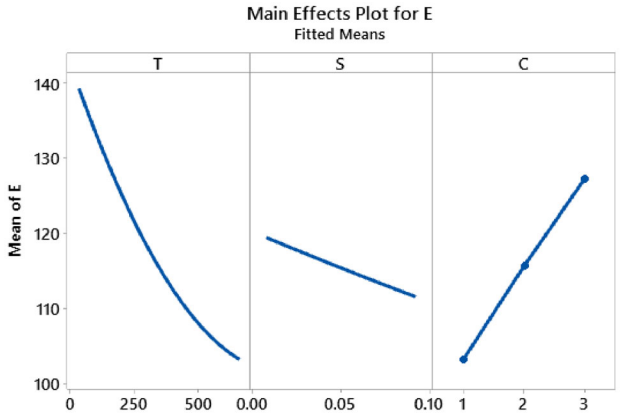

Fig. 6 Effect of temperature, strain rate and chirality on Young's modulus

According to the Table 7 related to Young's modulus, linear terms, quadratic, and overlap of input parameters are effective. According to P-value and F-value obtained from the analysis of variance, the linear terms of temperature, chirality and strain rate have the greatest effect on the Young's modulus, respectively. The quadratic terms of temperature, as well as the interaction between temperature and chirality also affect the Young's modulus. Also, according to Fig. 6, low levels of temperature and strain rate and the third type chirality increase the Young's modulus.

3.2.4 Optimization with the desirability approach

Derringer et al. [47] developed this approach which is a useful search-based optimization method for finding the optimal solutions globally. In this approach, each individual desirability function is assigned between one and zero for the outputs. Consequently, one indicates that the output is in full desirability and at its target. Zero, on the other hand, shows that the output is at the lowest desirability level [48, 49]. Therefore, the goal is to determine the values of the input variables in such a way that, firstly, for each output the desirability is greater than zero, secondly, the overall desirability is maximized. The purpose of optimization in this research is to maximize the ultimate stress and Young's modulus. Using Derringer method, the optimal parameters for simultaneous optimization of two the response outputs are determined. The result was obtained using Minitab software, which is shown in Fig. 7. In this figure, the first row indicates the input parameters, the range of their changes, and the optimal value of the parameter is located between its upper and lower limits. Also, the first column represents the value of the overall objective function, the objective function

Table 7 Analysis of Variance for the Young's modulus

Source	DF	Adj SS	Adj MS	*F*-Value	*P*-Value
Model	11	6721.05	611.00	1117.72	0.000
Linear	4	6579.55	1644.89	3009.01	0.000
T	1	2661.87	2661.87	4869.39	0.000
S	1	127.09	127.09	232.48	0.000
C	2	3790.59	1895.30	3467.08	0.000
Square	2	129.96	64.98	118.87	0.000
T × T	1	120.64	120.64	220.69	0.000
S × S	1	0.04	0.04	0.07	0.798
2-Way Interaction	5	11.54	2.31	4.22	0.006
T × S	1	0.76	0.76	1.39	0.249
T × C	2	10.74	5.37	9.82	0.001
S × C	2	0.04	0.02	0.04	0.964
Error	27	14.76	0.55		
Total	38	6735.81			
R-sq = 99.78%, R-sq(adj) = 99.69%					

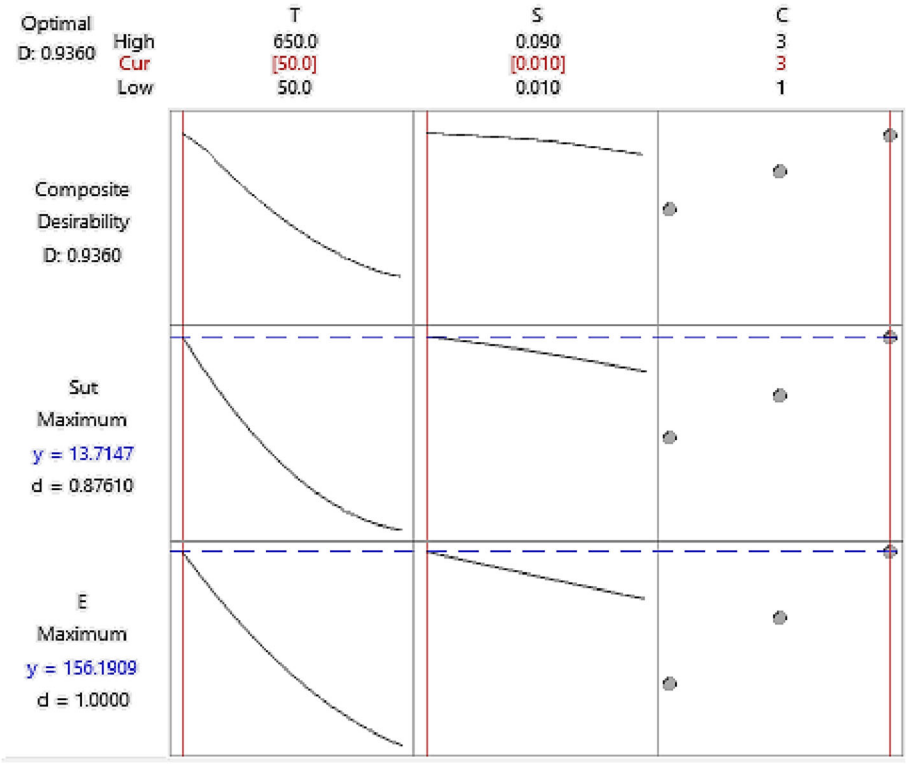

Fig. 7 The optimal ultimate stress and Young's modulus using the Derringer method

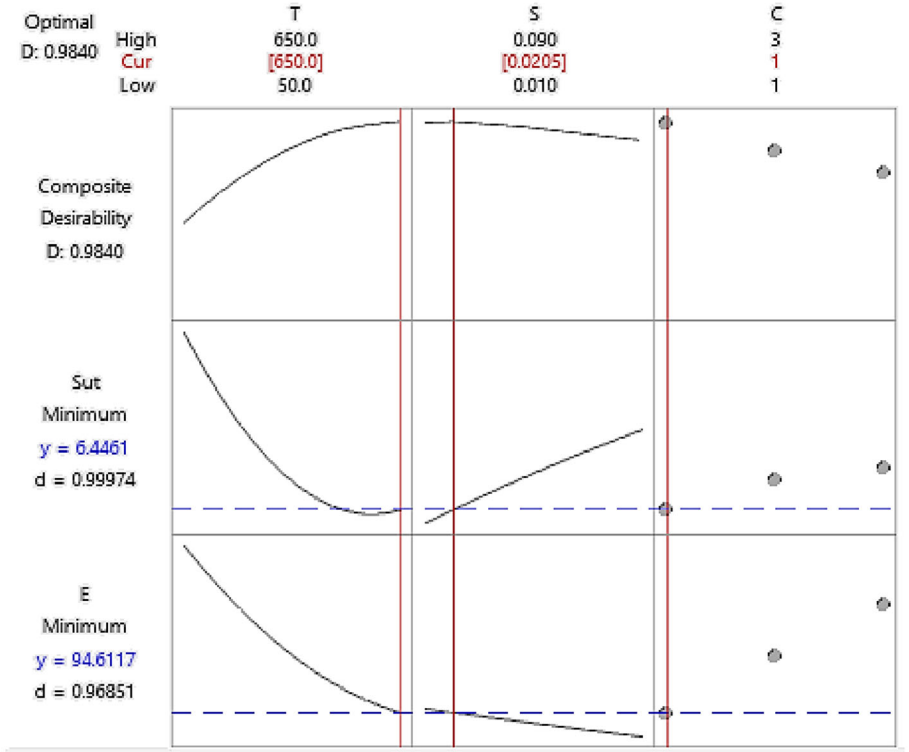

Fig. 8 Simultaneous minimum values of ultimate stress and Young's modulus

of each of the response variables, and the optimal value of the response variable. In addition, each of the cells in the figure describes how the response variable changes with respect to the change of one parameter while the other parameters are stable. Also, in Fig. 7, the red vertical line in each cell shows the value of the optimal input parameter and the blue dashed line shows the value of the optimal response variable. It can be concluded that the optimal conditions are created simultaneously at 50 K, strain rate 0.01, and the third type of chirality, in which the value of the elastic modulus is 156 GPa and the ultimate stress value is 13.7 GPa.

Also, according to Fig. 8, simultaneous minimum values of ultimate stress and Young's modulus occur at 650 K, strain rate 0.0205 and the first type of chirality.

4 Conclusion

In this study, first, the mechanical properties of aluminum/carbon AL/CNT nanotube nanocomposite were investigated, and the effect of temperature change, strain rate, and chirality of nanotubes on the elastic modulus and ultimate stress of the nanocomposite was investigated. The results indicated that, with increasing temperature, the Young's modulus value decreases, but the ultimate stress cannot be commented.

However, in order to simultaneously study these 3 parameters on the properties of nanocomposites, and find an optimal point for the elastic modulus and ultimate stress, the experimental design method was used for optimization. Using Derringer method, the optimal parameters for simultaneous optimization of two response variables, namely elastic modulus and final stress, were determined. It can be concluded that the optimal conditions are created simultaneously at a temperature of 50 K, a strain rate of 0.01 and chirality (5,5), in which the value of the elastic modulus is 156 GPa and the final stress value is 13.7 GPa, and simultaneous minimum values of ultimate stress and Young's modulus occur at 650 K, strain rate 0.0205, and chirality (3,3), in which case the value of elastic modulus is 94 GPa and final stress is 6.44 GPa.

Authors' contributions All authors contributed to the design and implementation of the research, to the analysis of the results, and to the writing of the manuscript.

Funding No funding to declare.

Data availability The data that support the findings of this study are available from the corresponding author.

Code availability The LAMMPS package is free and open-source software.

Declarations

Conflict of interest The authors declare that there is no conflict of interest.

References

1. Kelly A (1985) Composites in context. Compos Sci Technol 23(3):171–199
2. Thostenson ET, Li C, Chou TW (2005) Nanocomposites in context. Compos Sci Technol 65(3–4):491–516
3. Camargo PHC, Satyanarayana KG, Wypych F (2009) Nanocomposites: synthesis, structure, properties and new application opportunities. Mater Res 12(1):1–39
4. Komarneni S (1992) Nanocomposites. J Mater Chem 2(12):1219–1230
5. Tsai PC, Jeng YR, Lee JT, Stachiv I, Sittner P (2017) Effects of carbon nanotube reinforcement and grain size refinement mechanical properties and wear behaviors of carbon nanotube/copper composites. Diam Relat Mater 74:197–204
6. Bakshi SR, Lahiri D, Agarwal A (2010) Carbon nanotube reinforced metal matrix composites-a review. Int Mater Rev 55(1):41–64
7. Burkholder GL, Kwon YW, Pollak RD (2011) Effect of carbon nanotube reinforcement on fracture strength of composite adhesive joints. J Mater Sci 46(10):3370–3377
8. Park YG, Min H, Kim H, Zhexembekova A, Lee CY, Park JU (2019) Three-dimensional, high-resolution printing of carbon nanotube/liquid metal composites with mechanical and electrical reinforcement. Nano Lett 19(8):4866–4872
9. Carreño-Morelli E, Yang J, Couteau E, Hernadi K, Seo JW, Bonjour C, Schaller R (2004) Carbon nanotube/magnesium composites. Physica Status Solidi 201(8):R53–R55
10. Ni X, Furtado C, Fritz NK, Kopp R, Camanho PP, Wardle BL (2020) Interlaminar to intralaminar mode I and II crack bifurcation due to aligned carbon nanotube reinforcement of aerospace-grade advanced composites. Compos Sci Technol 190:108014
11. Li Q, Viereckl A, Rottmair CA, Singer RF (2009) Improved processing of carbon nanotube/magnesium alloy composites. Compos Sci Technol 69(7–8):1193–1199
12. Uddin SM, Mahmud T, Wolf C, Glanz C, Kolaric I, Volkmer C, Fecht HJ (2010) Effect of size and shape of metal particles to improve hardness and electrical properties of carbon nanotube reinforced copper and copper alloy composites. Compos Sci Technol 70(16):2253–2257
13. Silvestre N (2013) State-of-the-art review on carbon nanotube reinforced metal matrix composites. Int J Compos Mater 3(6):28–44
14. Kuzumaki T, Ujiie O, Ichinose H, Ito K (2000) Mechanical characteristics and preparation of carbon nanotube fiber-reinforced Ti composite. Adv Eng Mater 2(7):416–418
15. Tjong SC (2013) Recent progress in the development and properties of novel metal matrix nanocomposites reinforced with carbon nanotubes and graphene nanosheets. Mater Sci Eng R Rep 74(10):281–350
16. Esawi AM, Morsi K, Sayed A, Gawad AA, Borah P (2009) Fabrication and properties of dispersed carbon nanotube–aluminum composites. Mater Sci Eng A 508(1–2):167–173
17. Liu ZY, Xiao BL, Wang WG, Ma ZY (2012) Singly dispersed carbon nanotube/aluminum composites fabricated by powder metallurgy combined with friction stir processing. Carbon 50(5):1843–1852

18. Kim IY, Lee JH, Lee GS, Baik SH, Kim YJ, Lee YZ (2009) Friction and wear characteristics of the carbon nanotube–aluminum composites with different manufacturing conditions. Wear 267(1–4):593–598
19. Wu J, Zhang H, Zhang Y, Wang X (2012) Mechanical and thermal properties of carbon nanotube/aluminum composites consolidated by spark plasma sintering. Mater Des 41:344–348
20. Chen B, Kondoh K, Imai H, Umeda J, Takahashi M (2016) Simultaneously enhancing strength and ductility of carbon nanotube/aluminum composites by improving bonding conditions. Scripta Mater 113:158–162
21. Izadi H, Gerlich AP (2012) Distribution and stability of carbon nanotubes during multi-pass friction stir processing of carbon nanotube/aluminum composites. Carbon 50(12):4744–4749
22. Liu ZY, Xiao BL, Wang WG, Ma ZY (2014) Analysis of carbon nanotube shortening and composite strengthening in carbon nanotube/aluminum composites fabricated by multi-pass friction stir processing. Carbon 69:264–274
23. Bakshi SR, Agarwal A (2011) An analysis of the factors affecting strengthening in carbon nanotube reinforced aluminum composites. Carbon 49(2):533–544
24. Salama EI, Abbas A, Esawi AM (2017) Preparation and properties of dual-matrix carbon nanotube-reinforced aluminum composites. Compos A Appl Sci Manuf 99:84–93
25. Hassan MT, Esawi AM, Metwalli S (2014) Effect of carbon nanotube damage on the mechanical properties of aluminium–carbon nanotube composites. J Alloy Compd 607:215–222
26. Park JG, Keum DH, Lee YH (2015) Strengthening mechanisms in carbon nanotube-reinforced aluminum composites. Carbon 95:690–698
27. Yan Y, Lei Y, Liu S (2018) Tensile responses of carbon nanotubes-reinforced copper nanocomposites: molecular dynamics simulation. Comput Mater Sci 151:273–277
28. Motamedi M, Naghdi A, Jalali K (2010) Effect of temperature on properties of aluminum/single-walled carbon nanotube nanocomposite by molecular dynamics simulation. Proc IMechE Part C J Mech Eng Sci. https://doi.org/10.1177/0954406219878760
29. Motamedi M (2020) A space structural mechanics model of silicene. Proc Inst Mech Eng Part N J Nanomat Nanoeng Nanosyst 23:977
30. Motamedi M, Eskandari M, Yeganeh M (2012) Effect of straight and wavy carbon nanotube on the reinforcement modulus in nonlinear elastic matrix nanocomposite. Mater Des 34:603–608
31. Silvestre N, Faria B, Lopes JNC (2014) Compressive behavior of CNT-reinforced aluminum composites using molecular dynamics. Compos Sci Technol 90:16–24
32. Stuart SJ, Tutein AB, Harrison JA (2000) A reactive potential for hydrocarbons with intermolecular interactions. J Chem Phys 112(14):6472–6486
33. Wei Y, Wu J, Yin H, Shi X, Yang R, Dresselhaus M (2012) The nature of strength enhancement and weakening by pentagon–heptagon defects in graphene. Nat Mater 11(9):759–763
34. Bashirvand S, Montazeri A (2016) New aspects on the metal reinforcement by carbon nanofillers: a molecular dynamics study. Mater Des 91:306–313
35. Yishi S et al (2014) Computational structural modeling and mechanical behavior of carbon nanotube reinforced aluminum matrix composites. Mater Sci Eng A 614:273–283
36. Choi BK, Yoon GH, Lee S (2015) Molecular dynamics studies of CNT-reinforced aluminum composites under uniaxial tensile loading. Compos Part B. https://doi.org/10.1016/j.compositesb.2015.12.031
37. Laha T et al (2009) Tensile properties of carbon nanotube reinforced aluminum nanocomposite fabricated by plasma spray forming. Compos A App Sci Manuf 40(5):589–594
38. Choi HJ, Shin JH, Bae DH (2012) The effect of milling conditions on microstructures and mechanical properties of AL/MWCNT composites. Compos A App Sci Manuf 43(7):1061–1072
39. Deng CF et al (2007) Processing and properties of carbon nanotubes reinforced aluminum composites. Mater Sci Eng A 444(1–2):138–145
40. Esawi A et al (2010) Effect of carbon nanotube (CNT) content on the mechanical properties of CNT-reinforced aluminium composites. Compos Sci Technol 70:2237–2241
41. Bayar S, Delale F, Liaw M (2014) Effect of temperature on mechanical properties of Nanoclay-reinforced polymeric nanocomposites. I: experimental results. J Aerosp Eng 27:491–504
42. Singh A, Kumar D (2018) Effect of temperature on elastic properties of CNT-polyethylene nanocomposite and its interface using MD simulations. J Mol Model 24:178
43. Jun H, Zhirong D, Chen S, Qinlong L (2017) Molecular dynamics study on the tensile properties of graphene/Cu nanocomposite. Int J Comput Mater Sci Eng 6(2):1750021
44. Moeini M et al (2020) Molecular dynamics simulations of the effect of temperature and strain rate on mechanical properties of graphene–epoxy nanocomposites. Mol Simul 46(6)
45. Myers RH, Montgomery DC (1995) Response surface methodology: process and product optimization using designed experiments. Wiley, New York
46. Mehrvar A, Basti A, Jamali A (2020) Inverse modelling of electrochemical machining process using a novel combination of soft computing methods. Proc IMechE Part C J Mech Eng Sci 234(17):3436–3446
47. Derringer G, Suich R (1980) Simultaneous optimization of several response variables. J Qual Technol 12:214–219
48. Castillo ED, Montgomery DC, Mc Carville DR (1996) Modified desirability functions for multiple response optimizations. J Qual Technol 28(3):337–345
49. Mehrvar A, Basti A, Jamali A (2017) Modelling and parameter optimization in electrochemical machining process: application of dual response surface-desirability approach. Lat Am Appl Res 47(4):157–162